This article has been accepted for publication in IEEE Control Systems Letters. This is the author's version which has not been fully edited and content may change prior to final publication. Citation information: DOI 10.1109/LCSYS.2024.3496814

Tuning of Real-Time Optimization of Heliostat Concentrated Solar Power

Zachary Bernius[†‡], Claus Danielson[‡], Haden Harper[†‡], Ken Armijo[†]

***Abstract*— This paper investigates a real-time optimization algorithm for autonomously calibrating the heliostats in a concentrated solar power plant to maximize power generation. The current state-of-the-art uses open-loop control with human-operators to provide feedback on the heliostats. This paper presents a method for tuning the RTO to ensure stable and fast convergence to the optimal alignment, which is robust to uncertainty in the shape of the sunspot. The exponential stability of the system is certified using a quadratic Lyapunov function and output feedback methods to couple the Lyapunov functions of the plant and the Real-Time Optimization (RTO) algorithm. To validate stability, performance, and robustness, the closed-loop system is simulated using different power distributions that demonstrate the need for our RTO algorithm.**

***Index Terms*— Closed-loop control, Heliostat control, Real-time optimization**

I. Introduction

Concentrated Solar Power (CSP) is a reliable form of renewable energy that can rival non-renewable sources [7] in energy production and operation costs. A CSP plant concentrates solar energy to heat a working fluid used in a traditional thermodynamic cycle to produce electricity [12]. Although the power capacity varies with the time of day and year, CSP power remains available year-round and over-night using thermal storage. While there are several different methods of CSP [11] [9], the focus of this paper is on CSP using heliostats. A heliostat is a collection of mirrors or facets that reflects sunlight onto a power tower, also known as the receiver, as a sunspot to heat the working fluid. The main challenge of CSP plant heliostats is that they require closed-loop control to remain aligned with the movement of the Sun. The theoretical Carnot efficiency of power generation increases with the heat-flux on the receiver; thus, to maximize power generation, the heliostats need to continually realign with the Sun's movement to reflect sunlight optimally onto the receiver. Ideally, this realignment can be performed autonomously using RTO [4] to find and maintain the optimal pointing alignment.

Currently, the desired alignment is provided by open-loop commands from a human-operator in the form of azimuth and elevation angles tracked by the heliostats. These set-points are computed using the current positions of the Sun, mirror, and receiver. This approach reduces power generation for several reasons. First, without feedback, model uncertainty introduces error, resulting in a misaligned sunspot on the receiver. This is introduced by differences in the blueprint and actual locations of the heliostat and miscalibrated encoders used by the inner-loop heliostat controllers. Second, the heliostats do not track the Sun's movement perfectly. Slight tracking errors accumulate over time, causing the sunspot to drift from its desired position, requiring a skilled operator to continuously monitor and adjust the heliostats' alignment, increasing operational costs. Third, disturbances, such as wind, can misalign the heliostats. This paper presents an RTO algorithm for autonomously aligning the CSP plant heliostats to maximize power generation despite model uncertainty and disturbances using real-time feedback.

Other methods have been proposed for real-time power maximization in CSP. system observation for heliostat orientations while tracking (SOHOT) is a commercial method that uses images of the heliostats and ray-tracing programs to calculate the heliostats' optimal pointing alignment [6]. However, this method is time-consuming and expensive. Furthermore, it does not address the need for autonomous feedback, instead provides more data to the operator, increasing their workload and the skill-level necessary to operate the CSP plant. There are also other closed-loop control approaches by Kribus et al. [5] and by Freeman et al. [3]. The method in [5] compares four images around the receiver to measure and use sunlight spillage as feedback to adjust the heliostat. The work in [3] builds upon [5] by perturbing the light waves picked up by photo-sensors around the receiver and calculating the heliostat's surface normal vector to improve calibration and standalone movement. Our method is distinct from previous approaches in that it uses real-time measurements combined with a gradient ascent to maximize power. A key advantage of our data-driven approach is its compatibility with various data collection methods commonly employed by existing CSP plants, which helps to lower installation and operational costs. Additionally, our method implicitly filters the sensor measurements to obtain a robust estimate of the heliostat's optimal pointing alignment, whereas other methods assume that the sensor measurements obtained by specialized sensors are ground-truth.

We contribute a semi-definite programming (SDP)-based algorithm for tuning the parameters of a standard RTO architecture [8] applied to the CSP alignment problem. Our tuning algorithm ensures exponential stability, minimal settling-time, and guaranteed robustness to model uncertainty. We exploit the Hammerstein structure and exponential nonlinearity of the CSP plant to transform the closed-loop system model into an uncertain linear system. This allows us to adapt SDP techniques for output-feedback to tune the RTO for performance and robustness. We formulate the SDP with linear matrix inequality (LMI) constraints that guarantee robust stability despite the unknown shape of the sunspot produced by the heliostat facets. We formulate the SDP cost to minimize the worst-case settling-time of the uncertain closed-loop system. This method can be applied to similar problems that have a similar Hammerstein structure with an exponential non-linearity.

[†] Sandia National Laboratories, [‡] University of New Mexico

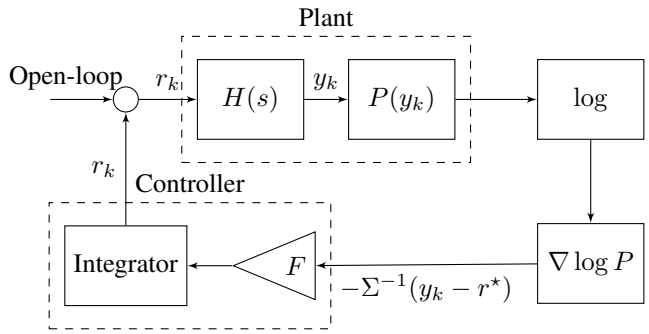

Fig. 1. Block diagram of the closed-loop RTO architecture for real-time optimization of heliostat CSP.

II. RTO Tuning Problem

In this section, we describe the heliostat alignment problem and the architecture of the RTO adapted to solve this problem. The block diagram of a heliostat-CSP in closed-loop with an RTO controller is shown in Fig. 1.

A. Plant Dynamics

The plant is modeled as a Hammerstein system consisting of the heliostat dynamics and a nonlinear power function. The heliostat is modeled as a known linear system with generic state-space realization

$$x_{k+1} = Ax_k + Br_k \tag{1a}$$
$$y_k = Cx_k \tag{1b}$$

where $x_k \in \mathbb{R}^n$ is the state at time k. The dynamics (1) are inherently multi-input/multi-output with the reference $r_k = (r_{k,az}, r_{k,el}) \in \mathbb{R}^2$ consisting of the desired azimuth r_{az} and elevation angle r_{el} of the heliostat, and the output $y_k = (y_{k,az}, y_{k,el}) \in \mathbb{R}^2$ consisting of the actual azimuth y_{az} and elevation angle y_{el}. The heliostats are servo-ed by an inner-loop controller that ensures that measured outputs $y \to r$ converge to the reference r. The RTO will find the reference r that maximizes power.

The intensity of light across the sunspot generated by the heliostat has a Gaussian distribution [10]

$$P(y) = \frac{\bar{P}}{\sqrt{(2\pi)^2|\Sigma|}} \exp\left(-\frac{1}{2}(y - r^*)^T \Sigma^{-1}(y - r^*)\right) \tag{2}$$

where $\bar{P}$ is the unknown power provided by the Sun, the unknown matrix $\Sigma^{-1} \in \mathbb{R}^{2\times 2}$ determines the shape of the sunspot, and the unknown optimal alignment $r^\star \in \mathbb{R}^2$ has a complicated dependence on the relative positions of the Sun, heliostat, and receiver.

The time-varying nominal power $\bar{P}_k$ is a source of multiplicative noise. By taking the logarithm of (2), we obtain $\log P(y) = \nu_k - \frac{1}{2}(y - r^\star)^T \Sigma^{-1}(y - r^\star)$ where $\nu_k = \log \bar{P}/\sqrt{(2\pi)^2|\Sigma|}$ is now an additive disturbance independent of y. Furthermore, when we take the gradient $\nabla_y \log P(y)$ of the log-power with respect to y, this term disappears. In practice, ν_k is slowly varying since fluctuations in the nominal power $\bar{P}_k$ are caused by the movement of the Sun or clouds which are slow relative to the heliostat bandwidth.

The shape matrix Σ^{-1} is the main source of uncertainty since the slowly varying disturbance ν_k and unknown optimal alignment $r^\star$ will be estimated from power measurements. We model this uncertainty as a convex-hull of the shape matrices Σ^{-1}

$$\mathcal{D} = \left\{ \sum_{i=1}^N \xi_i \Sigma_i^{-1} : \sum_{i=1}^N \xi_i = 1, \xi_i \geq 0 \right\} \tag{3}$$

The vertices Σ_i^{-1} of the set (3) are empirically identified from images of sunspots on the receiver. Our assumption is that in practice any encountered sunspot shape Σ^{-1} will lie within the convex-hull (3) of previously encountered sunspots.

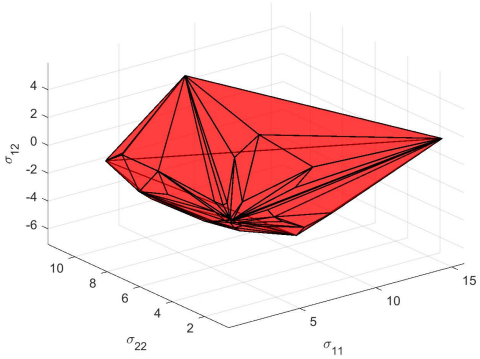

Fig. 2. Example illustrating of the convex-hull (3) of **100** realistic symmetric shape matrices $\boldsymbol{\Sigma^{-1}} \in \mathbb{R}^{\mathbf{2\times 2}}$. Axis are azimuth $\boldsymbol{\sigma_{11}}$ and elevation $\boldsymbol{\sigma_{22}}$ variances and their covariance $\boldsymbol{\sigma_{12}}$.

B. Gradient Estimator

Since the parameters of (2) are unknown, its gradient $\nabla \log P(y)$ is estimated from real-time power measurements $\log P_k = \log P(y_k)$ gathered at y_k over time k, creating the data-set $\{y_k, \log P_k\}$. Our RTO architecture is agnostic to the choice of gradient estimation algorithm, providing significant flexibility. This means our data can include various measurements such as temperature, heat flux, light intensity, or other metrics correlated with power generation.

C. RTO Algorithm

The RTO iteratively finds the optimal alignment $r^\star$ using gradient ascent which has the state-space dynamics

$$z_{k+1} = z_k + F\nabla \log P(y_k) \tag{4a}$$
$$\hat{r}_k = z_k \tag{4b}$$

where the RTO state $z_k = \hat{r}_k$ is the current estimate $\hat{r}_k$ of $r^\star$ supplied to the heliostat $r_k = \hat{r}_k$. For notational simplicity, we will use r_k to refer to these three equivalent signals. The RTO input is the gradient $\nabla \log P(y_k)$ at y_k. Since the logarithm of (2) is concave, the power is maximized when $\nabla \log P = 0$.

The objective of this paper is to tune the RTO (4) gain $F \in \mathbb{R}^{2\times 2}$. Since the RTO is a purely integral controller, it must be carefully tuned to prevent instability and ensure fast convergence to $r^\star$. This issue is exacerbated by the presences of the static nonlinear function (2) in the closed-loop, as shown

This article has been accepted for publication in IEEE Control Systems Letters. This is the author's version which has not been fully edited and content may change prior to final publication. Citation information: DOI 10.1109/LCSYS.2024.3496814

in Fig. 1. Additionally, we need to consider the parametric uncertainty (3) of Σ^{-1}, which can negatively effect stability and performance. This paper investigates the tuning of the gain F to provide exponential stability, minimize alignment time, and ensure robustness.

D. Control Objectives and Assumptions

This section formally defines the RTO tuning problem and our assumptions on this problem.

Problem 1. *Tune the gain $F \in \mathbb{R}^{2\times 2}$ of the* RTO (4) *to achieve the following control objectives:*

(a) Stabilize the closed-loop system shown in Fig. 1.
(b) Ensure that y_k converges $y_k \to r^\star$ to the optimal $r^\star$.
(c) Minimize the settling-time to reach the optimal $r^\star$.
(d) Ensure robustness to the parametric uncertainty (3)*.*

Our analysis is based on the following assumptions.

Assumption 1.

(a) The heliostat dynamics are Schur stable and have identity steady-state gain $C(I-A)^{-1}B = I$.
(b) The intensity of light across the sunspot has a Gaussian distribution (2)*.*
(c) The gradient $\nabla \log P(y_k)$ is estimated without error.
(d) The shape matrix Σ^{-1} belongs to the convex-hull (3)*.*

Assumption 1(a) is reasonable since the heliostats are controlled by an inner-loop controller that points the heliostats in the desired reference direction. Assumption 1(b) is consistent with experimental observations of the sunspot profile for heliostats with a single facet. However, errors in facet installation could result in multiple peaks in the sunlight intensity. Although Assumption 1(c) is unrealistic in practice, it was made so that our analysis can focus on the challenge of tuning F for convergence and robustness. This is a reasonable assumption since CSP plants tend to be well instrumented due to their expense in commissioning. Due to the ability to use many sensors, such as multiple thermocouples and millions of pixels in sunspot images, as well as a relatively large window to gather measurements due to the slow dynamics, we are typically estimating the gradient from millions of data-points.

III. Optimal Tuning of the RTO

In this section, we describe conditions on the gain F so that the RTO algorithm maximizes power, minimizes settling-time, and provides robustness to uncertainty.

A. Linearity of Closed-loop Dynamics

Our key insight is that the nonlinear system depicted in Fig. 1 is equivalent to a fully linear system under Assumption 1(d) since $\nabla \log P = -\Sigma^{-1}(y_k - r^\star)$ of the Gaussian log power distribution (2) reduces to an uncertain linear gain $-\Sigma^{-1}$ acting on y_k and $r^\star$. Thus, the three nonlinear blocks in Fig. 1 (the power function (2), the logarithm $\log P$, and gradient $\nabla \log P$) can be replaced by a linear gain block as shown in Fig. 3. This allows us to treat Σ^{-1} as an uncertain linear gain and $r^\star$ as a disturbance.

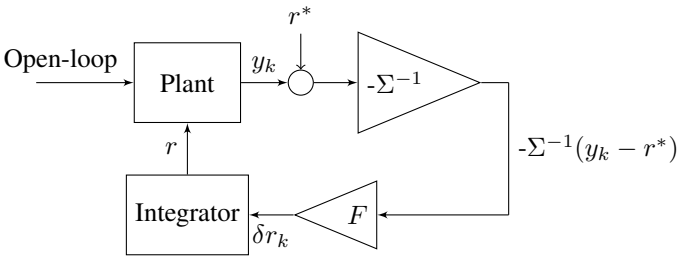

Fig. 3. Reduction of closed-loop block diagram in Fig. 1. Resulting closed-loop system is fully linear, but with uncertain gain $\boldsymbol{\Sigma^{-1}}$ and unknown optimal reference $\boldsymbol{r^\star}$.

For the linear system shown in Fig. 3, the dynamics of the closed-loop system have the state-space realization

$$\begin{bmatrix} x_{k+1} \\ r_{k+1} \end{bmatrix} = \begin{bmatrix} A & B \\ -F\Sigma^{-1}C & I \end{bmatrix} \begin{bmatrix} x_k \\ r_k \end{bmatrix} + \begin{bmatrix} 0 \\ F\Sigma^{-1} \end{bmatrix} r^* \tag{5}$$

obtained from (1), (4), and $\nabla \log P(y) = -\Sigma^{-1}(y - r^\star)$. The closed-loop state is comprised of x_k and $r_k = z_k$.

B. Condition for Optimal Pointing Alignment

In this section, we show that the equilibrium of (5) in Fig. 3 corresponds to $r^\star$ of the heliostat $y_\infty = r^\star$ through the following proposition.

Proposition 1. *Let Assumption 1 hold. Then, for any $F \neq 0$,*

$$(x_\infty, r_\infty) = ((I-A)^{-1}Br^*, r^*) \tag{6}$$

is the equilibrium of the system.

Proof: The equilibrium states of the heliostat x_∞ and RTO r_∞ satisfy the equilibrium condition

$$\begin{bmatrix} x_\infty \\ r_\infty \end{bmatrix} = \begin{bmatrix} A & B \\ -F\Sigma^{-1}C & I \end{bmatrix} \begin{bmatrix} x_\infty \\ r_\infty \end{bmatrix} + \begin{bmatrix} 0 \\ F\Sigma^{-1} \end{bmatrix} r^*$$

This produces the solutions $x_\infty = (I-A)^{-1}Br_\infty$ and $F\Sigma^{-1}C(I-A)^{-1}Br_\infty = F\Sigma^{-1}r^\star$. Since $C(I-A)^{-1}B = I$ by Assumption 1(a), this simplifies to $F\Sigma^{-1}r_\infty = F\Sigma^{-1}r^\star$. Thus, for $F \neq 0$, we have $r_\infty = r^\star$. □

Proposition 1 shows that any $F \neq 0$ satisfies control objective 1(b).

C. Convergence to Optimal Pointing Alignment

In this section, we show that there exists a F that stabilizes (5) to establish the feasibility of optimizing F.

Lemma 1. *Let Assumption 1 hold. Then, there exists a $F \succeq 0$ such that the equilibrium* (6) *is stable.*

The proof of Lemma 1 is provided in [1]. Lemma 1 shows that there exists a $F \succeq 0$ that satisfies control objective 1(a). The proof of Lemma 1 is constructive, using the small-gain theorem to produce $F = \frac{2}{\|\tilde{P}\|^2_{H_\infty}+2}\Sigma$. However, there are two issues with this gain. First, as we will illustrate in Section IV, this gain is conservative, producing slow convergence to $r^\star$. In the next section, we will present a method for tuning F to improve settling-time. Second, this gain depends on the unknown parameter Σ^{-1}. In Section III-E, we will show how to design F for robustness to Σ^{-1}. Nonetheless, Lemma 1 establishes that the RTO tuning problem is always feasible.

D. Tuning the RTO to Minimize Alignment Time

In this section, we pose the tuning of the gain F to minimize alignment time as an LMI where Σ is known. This will be extended to the uncertain case in the sequel. The closed-loop dynamics (5) can be factorized around F to produce

$$x_{k+1} = \left(\begin{bmatrix} A & B \\ 0 & I \end{bmatrix} + \begin{bmatrix} 0 \\ I \end{bmatrix} F \begin{bmatrix} -\Sigma^{-1}C & 0 \end{bmatrix} \right) x_k. \quad (7)$$

Thus, the closed-loop dynamics (5) can be re-interpreted as output feedback with the open-loop state-space realization

$$\left[\begin{array}{c|c} \hat{A} & \hat{B} \\ \hline \hat{C} & 0 \end{array}\right] = \left[\begin{array}{cc|c} A & B & 0 \\ 0 & I & I \\ \hline -\Sigma^{-1}C & 0 & 0 \end{array}\right] \quad (8)$$

The following lemma adapts the output feedback LMIs from [2] to tune the exponential convergence rate α provided by RTO gain F.

Lemma 2. *Let Assumption 1 hold and let Σ be known. If the scalar $\alpha \in [0, 1)$, symmetric positive definite matrix $S \in \mathbb{R}^{6\times6}$, and matrices $G \in \mathbb{R}^{6\times6}$, $V \in \mathbb{R}^{2\times2}$, and $U \in \mathbb{R}^{2\times2}$ satisfy the* LMI

$$\begin{bmatrix} \alpha(G + G^T - S) & (\hat{A}G + \hat{B}U\hat{C})^T \\ (\hat{A}G + \hat{B}U\hat{C}) & S \end{bmatrix} \succeq 0 \quad (9a)$$

and

$$V\hat{C} = \hat{C}G \quad (9b)$$

then the RTO *gain*

$$F = UV^{-1} \quad (9c)$$

exponentially stabilizes the closed-loop system (5).

Proof: We will show closed-loop stability using a quadratic Lyapunov function $V(x) = x^T P x$ where $P = S^{-1} \succ 0$. We will show that (9) implies the exponential stability condition $\Delta V(x_k) = x_{k+1}^T P x_{k+1} - \alpha x_k^T P x_k \leq 0$.

Substituting $FV = U$ and $V\hat{C} = \hat{C}G$ from (9c) and (9b) respectively into the LMI (9a) and using the condition $G^T S^{-1} G \succeq G^T + G - S$ from [2], we obtain

$$\begin{bmatrix} \alpha(G^T S^{-1} G) & G^T(\hat{A} + \hat{B}F\hat{C})^T \\ (\hat{A} + \hat{B}F\hat{C})G & S \end{bmatrix} \succeq 0$$

which can be re-written as

$$\begin{bmatrix} G^T & 0 \\ 0 & I \end{bmatrix} \begin{bmatrix} \alpha S^{-1} & (\hat{A} + \hat{B}F\hat{C})^T \\ (\hat{A} + \hat{B}F\hat{C}) & S^{-1} \end{bmatrix} \begin{bmatrix} G & 0 \\ 0 & I \end{bmatrix} \succeq 0.$$

Since $I \succeq 0$ and G is full-rank, this matrix is positive semi-definite if and only if

$$\begin{bmatrix} \alpha S^{-1} & (\hat{A} + \hat{B}F\hat{C})^T \\ (\hat{A} + \hat{B}F\hat{C}) & S \end{bmatrix} \succeq 0$$

Taking the Schur complement and substituting $P = S^{-1} \succ 0$, the LMI above produces the Lyapunov inequality

$$\alpha P - (\hat{A} + \hat{B}F\hat{C})^T P (\hat{A} + \hat{B}F\hat{C}) \succeq 0$$

Pre and post multiplying by the closed-loop state $\hat{x}_k = (x_k, r_k)$ produces the Lyapunov decrease condition

$$\Delta V(\hat{x}_k) = \hat{x}_k^T (\hat{A} + \hat{B}F\hat{C})^T P (\hat{A} + \hat{B}F\hat{C}) \hat{x}_k - \alpha \hat{x}_k^T P \hat{x}_k \leq 0$$

which implies that the closed-loop system (5) is exponentially stable with decay rate α. □

Lemma 2 provides a convex characterization of gains $F = UV^{-1}$ that exponentially stabilize (5). The exponential decay factor $\alpha \in [0, 1) \subset \mathbb{R}$ can be interpreted as the slowest pole of (5) and determines the rate at which the RTO drives the heliostat to the optimal $r^\star$. This convergence rate can be optimized using the following optimization problem

$$\min \quad \alpha^2 \quad (10a)$$

$$\text{s.t.} \quad S \succ 0, \ (9). \quad (10b)$$

Although the optimization problem (10) is non-convex in both α and S, we can use a line-search to iteratively optimize α. Therefore, Lemma 2 and (10) satisfy control objective 1(c).

It is tempting to simplify the tuning problem (9) by setting $G = S$. However, as the following proposition shows, this simplification is infeasible.

Proposition 2. *If $G = S$ then $\alpha = 1$ and $F = 0$ is the only feasible solution of* (9).

Proof: Consider partitioning the Lyapunov matrix S into

$$S = \begin{bmatrix} S_{11} & S_{12} \\ S_{12}^T & S_{22} \end{bmatrix} \succ 0$$

where the partitions S_{11} and S_{22} correspond to the plant and RTO dynamics, respectively, and S_{12} corresponds to the coupling in the closed-loop dynamics (5). Using the substitutions $BUC = BFCS$ from the proof of Lemma 2, the Schur complement of (9a) with $G = S$ is

$$0 \preceq \alpha S - (\hat{A} + \hat{B}F\hat{C})S(\hat{A} + \hat{B}F\hat{C})^T =$$
$$\begin{bmatrix} * & * \\ * & (\alpha - 1)S_{11} + FCS_{12} + (FCS_{12})^T - FCS_{11}(FC)^T \end{bmatrix}$$

where the terms $*$ are inconsequential for this proof. From (9b), we have $[V\Sigma^{-1}C, 0] = [\Sigma^{-1}CS_{11}, CS_{12}]$, which implies that $CS_{12} = 0$ since Σ^{-1} is positive definite. Thus, (9a) holds for $G = S$ if and only if the inequality $FCS_{11}C^T F^T \preceq (\alpha - 1)S_{11}$ holds i.e. the positive semi-definite matrix $FCS_{11}C^T F^T \succeq 0$ must be less than or equal to the negative semi-definite matrix $(\alpha - 1)S_{11} \preceq 0$ where $\alpha \leq 1$ and $S_{11} \succ 0$. This can only hold if these matrices are zero i.e. $\alpha = 0$ so that $(\alpha - 1)S_{11} = 0$ and $F = 0$ so that $FCS_{11}C^T F^T = 0$. □

Proposition 2 demonstrates the necessity of optimizing over the matrix $G \neq S$ in Lemma 2. A straightforward corollary of Proposition 2 is that Lyapunov function requires non-zero coupling $S_{12} = S_{21}^T \neq 0$ between the heliostat and RTO dynamics. Intuitively, this is necessary since the heliostat state x_k will diverge $x_k \not\to x_\infty(r_k)$ from its reference dependent equilibrium $x_\infty(r_k)$ when the RTO is aggressively converging to its equilibrium $r_k \to r^\star$. Likewise, the reference may diverge to drive the heliostat state closer to equilibrium. The coupling $S_{12} = S_{21}^T \neq 0$ in the Lyapunov matrix S accounts for the interaction between the heliostat and RTO dynamics.

E. Tuning the RTO for Robustness

For robustness, we need to tune F to stabilize (5) for all shape matrices Σ^{-1} contained in the uncertainty set (3). The following theorem ensures robust exponential stability.

Theorem 1. *Let Assumption 1 hold. If the scalar $\alpha \in [0,1)$, symmetric positive definite matrix $S \in \mathbb{R}^{6\times 6}$, and matrices $G_i \in \mathbb{R}^{6\times 6}$, $V \in \mathbb{R}^{2\times 2}$, and $U \in \mathbb{R}^{2\times 2}$ satisfy the* LMIs

$$\begin{bmatrix} \alpha(G_i + {G_i}^T - S) & (\hat{A}G_i + \hat{B}U\hat{C}_i)^T \\ (\hat{A}G_i + \hat{B}U\hat{C}_i) & S \end{bmatrix} \succeq 0 \tag{11a}$$

and

$$V\hat{C}_i = \hat{C}_i G_i \tag{11b}$$

for $i = 1, \ldots, N$, where $\hat{C}_i = \begin{bmatrix}\Sigma_i^{-1}C & 0\end{bmatrix}$, then the RTO *gain* (9c) *exponentially stabilizes the closed-loop system* (5) *for all Σ^{-1} in the set* (3)*.*

Proof: Consider the LMIs (11a) for the vertices Σ_i^{-1} of the uncertainty set (3)

$$\begin{bmatrix} \alpha(G_i + {G_i}^T - S) & (\hat{A}G_i + \hat{B}U\hat{C}_i)^T \\ (\hat{A}G_i + \hat{B}U\hat{C}_i) & S \end{bmatrix} \succeq 0.$$

Following similar arguments as the proof of Theorem 2, the matrix above is positive semi-definite if and only if

$$\begin{bmatrix} \alpha S^{-1} & (\hat{A} + \hat{B}F\hat{C}_i)^T \\ (\hat{A} + \hat{B}F\hat{C}_i) & S \end{bmatrix} \succeq 0.$$

By definition, any shape matrix Σ^{-1} in the convex-hull (3) can be parameterized as $\Sigma(\xi)^{-1} = \sum_{i=1}^N \xi_i \Sigma_i^{-1}$ where Σ_i^{-1} are the vertices of (3) and $\xi_i \geq 0$ and $\sum_{i=1}^N \xi_i = 1$. Applying the convex combination ξ to the inequality above produces

$$\sum_{i=1}^N \xi_i \begin{bmatrix} \alpha S^{-1} & (\hat{A} + \hat{B}F\Sigma_i^{-1}\hat{C})^T \\ \hat{A} + \hat{B}F\Sigma_i^{-1}\hat{C} & S \end{bmatrix}$$
$$= \begin{bmatrix} \alpha S^{-1} & \left(\hat{A} + \hat{B}F\Sigma(\xi)^{-1}\hat{C}\right)^T \\ \left(\hat{A} + \hat{B}F\Sigma(\xi)^{-1}\hat{C}\right) & S \end{bmatrix} \succeq 0$$

for the parameterized element $\Sigma(\xi)^{-1}$ of the convex-hull (3). Taking the Schur complement and substituting $P = S^{-1} \succ 0$, we obtain the Lyapunov inequality

$$\alpha P - (\hat{A} + \hat{B}F\Sigma^{-1}\hat{C})^T P (\hat{A} + \hat{B}F\Sigma^{-1}\hat{C}) \succeq 0$$

which holds for any shape matrix Σ^{-1} in the convex-hull (3). Thus, the closed-loop system is exponentially stable with decay rate α for all Σ^{-1} contained in the set (3). □

Theorem 1 shows that if the gain F satisfies (11) then it will satisfy control objective 1(d). The conditions (11) exploit convexity to reduce the infinite number of constraints imposed by the uncertainty set (3) to a finite number of LMIs.

IV. Simulations and Results

In this section, we will compare convergence rates of the optimized F with the conservative gain presented in Lemma 1 and the robustness of F tuned using (11) with non-robust optimization-based tuning (9).

A. Numerical Details

In this section, we numerically define the parameters used in the simulations.

1) Heliostat Dynamics: The heliostat dynamics (1) are modeled by the transfer matrix

$$H(s) = \begin{bmatrix} H_{az,az}(s) & H_{az,el}(s) \\ H_{el,az}(s) & H_{el,el}(s) \end{bmatrix}$$

where azimuth and elevation dynamics are uncoupled $H_{az,el}(s) = H_{el,az}(s) = 0$. The dynamics $H_{az,az}(s)$ and $H_{el,el}(s)$ are second-order with transfer functions

$$H_i(s) = \frac{{\omega_n}^2}{s^2 + 2\zeta\omega_n s + {\omega_n}^2 + {\omega_n}^2}$$

for both azimuth $i = az, az$ and elevation $i = el, el$, where $\zeta_{az} = 1.1$, $\zeta_{el} = 1.05$, $\omega_{n,az} = \frac{1}{10}$, and $\omega_{n,el} = \frac{1}{20}$. Since $\zeta_{az} > \zeta_{el} = 1.05 > 1$, the dynamics are over-damped, reflecting the typical design of the inner-loop servos on the heliostats. The natural frequencies ω_n were chosen to represent the typical settling times observed for the heliostats moving in each direction. The values ζ and ω_n differ between each direction to simulate possible differences between the azimuth and elevation angle transfer functions. The heliostat model $H(s)$ was converted into a discrete-time state-space with sample period 6 seconds. For each simulation, $r_0 \neq r^\star$ is the alignment provided by the operator. However, this alignment is non-optimal due to uncertainty about the heliostat position and encoder errors.

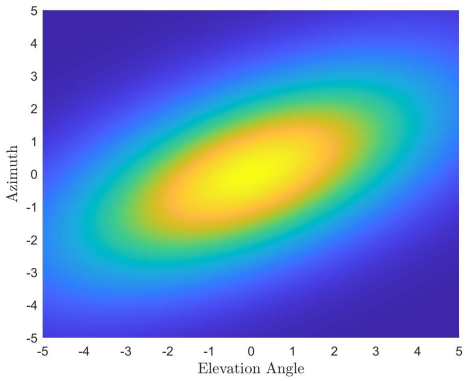

Fig. 4. Oblong Power Distribution. This figure shows the power intensity $\boldsymbol{P(y)}$ at a given $\boldsymbol{y_{az}}$ and $\boldsymbol{y_{el}}$.

2) Power Distributions: The power distribution in Fig. 4 is used to simulate the RTO algorithm, where $\Sigma = \begin{bmatrix} 10 & 4 \\ 4 & 5 \end{bmatrix}$ is used to simulate the RTO algorithm. $r^\star = (0,0)$ and maximum power intensity $P(r^\star) = 100\%$ are known in order to validate the RTO algorithm. These choices are made without loss of generality to ensure the clarity of the plots. In practice, $r^\star$ and $P(r^\star)$ will be unknown.

3) Gradient Estimator: For our simulations, a batch least squares (BLS) algorithm was used to estimate $\nabla \log P(y_k)$. Using the first-order Taylor series expansion $\log P_i \approx \log P(y_k) + \nabla \log P(y_k)^T (y_i - y_k) = \theta^T \phi_i$ where $\theta = (\log P(y_k), \nabla \log P(y_k))$ is the parameter vector and $\phi_i = (1, y_i - y_k)$ is the regressor vector. The parameters θ are estimated using the BLS estimator $\hat{\theta} = (\Phi\Phi^T)^{-1}\Phi P$ where $\Phi = \begin{bmatrix}\phi_1 & \ldots & \phi_N\end{bmatrix}$ is the batch regressor matrix and $P =$

This article has been accepted for publication in IEEE Control Systems Letters. This is the author's version which has not been fully edited and content may change prior to final publication. Citation information: DOI 10.1109/LCSYS.2024.3496814

$\begin{bmatrix} P_1 & \dots & P_N \end{bmatrix}^T$ is the batch output vector with N measurements. $\nabla \log P(y_k)$ is pulled from the vector $\hat{\theta}$. In the simulations, $\nabla \log P(y_k)$ was estimated using 10 sensors in a circular configuration with radius 0.1 around each y_k.

4) RTO design: The gain F of the controller (4) used in the next section was calculated using Σ^{-1} from the power distribution in Fig. 4 and Theorem 2. The computation was performed in 1.668338 seconds using the MATLAB package Yalmip with the SDPT3 solver. This solver was used to solve the SDP problem (10) where (9a) $\in \mathbb{R}^{12\times 12}$. The optimal $\alpha = 0.9999999$, which is the smallest value for which (10) is feasible, was found via line-search.

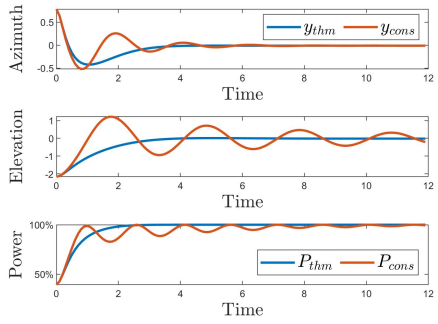

Fig. 5. Simulations with Conservative (red) and Theorem 2 (blue) gains. These simulations shows $(\boldsymbol{y_{az}, y_{el}})$ versus time (top and middle, respectively) and $\boldsymbol{P(y)}$ versus time (bottom).

5) Simulations: Fig. 5 shows the simulation results for the nonlinear closed-loop system shown in Fig. 1 using the conservative gain suggested by Lemma 1 (left) and the gain from Theorem 2 (right). Fig. 4 shows the distribution (2) used in these simulations.

Fig. 5 shows the time-varying y_k of the heliostat (1) using the conservative gain from Lemma 1 and the gain from Theorem 2. For each simulation, y_k converges to $r^\star$ $y_k \to r_k \to 0$. In Fig. 5, we see oscillator closed-loop behavior due to the interaction of the dynamic systems (1) and (4). This shows that this is not a simple gradient ascent problem and justifies the need for careful analysis of the non-trivial closed-loop dynamics. Fig. 5 also shows that the power $P_k = P(y_k)$ converges $P_k \to 100\%$ to the maximum power $\bar{P} = 100\%$. The heliostat converged to the optimal alignment in 2 minutes for the optimized gain, but 9 minutes for the conservative gain.

These simulations empirically validate Proposition 1 and Lemma 1. The simulations also empirically validate Lemma 2, proving the Lemma 2 F stabilizes the closed-loop system in Fig. 1 and settles faster than the conservative Lemma 1 gain.

Fig. 6 shows the robust simulation results for the nonlinear closed-loop system shown in Fig. 1 comprised of the heliostat (1), Gaussian power distribution (2), and RTO (4). For these simulations, 25 different shape matrices Σ^{-1} were randomly drawn from the uncertainty set (3). Then, each Σ was simulated using the robust gain and non-robust gain with the same initial conditions. Fig. 6 show the alignment y_k of the heliostat (1). For each of the 25 power distribution (2), the alignment y_k converges $y_k \to r_k \to r^\star = 0$ to the optimal

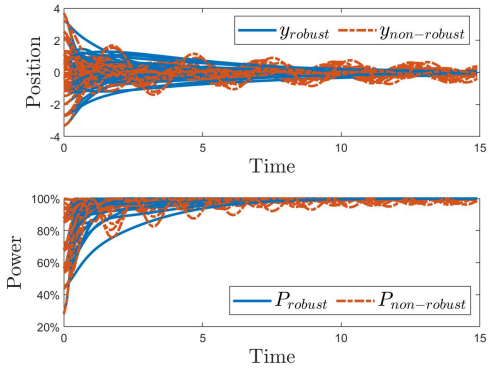

Fig. 6. Robust Simulations with Robust (blue) and Non-robust (red) gains. This simulation shows $(\boldsymbol{y_{az}, y_{el}})$ versus time (top). The simulation also shows $\boldsymbol{P(y)}$ versus time (bottom).

$r^\star = 0$. Fig. 6 shows that the power $P_k = P(y_k)$ converges $P_k \to \bar{P} = 100\%$ to the maximum power $\bar{P} = 100\%$ for each power distribution.

These simulations empirically validate Lemma 1 by showing a reduction in alignment time using the optimized F. Furthermore, these simulations empirically demonstrate robustness to the uncertainty (3) proven in Theorem 1; for each random Σ^{-1}, the optimized F ensured robust convergence.

REFERENCES

[1] Zachary Bernius. Tuning of real-time optimization of heliostat concentrated solar power. Master's thesis, University of New Mexico, 2024.

[2] J. Daafouz, P. Riedinger, and C. Iung. Stability analysis and control synthesis for switched systems: a switched lyapunov function approach. *IEEE Transactions on Automatic Control*, 47(11):1883–1887, 2002.

[3] Joshua Freeman, Keerthi K. S, and Lekshmi R. Chandran. Closed loop control system for a heliostat field. In *2015 International Conference on Technological Advancements in Power and Energy (TAP Energy)*, pages 272–277, 2015.

[4] Ali Kashani, Shirin Panahi, Ankush Chakrabarty, and Claus Danielson. Robust data-driven dynamic optimization using a set-based gradient estimator. *Optimal Control Applications and Methods*, 06 2024.

[5] Abraham Kribus, Irina Vishnevetsky, Amnon Yogev, and Tatiana Rubinov. Closed loop control of heliostats. *Energy*, 29(5):905–913, 2004. SolarPACES 2002.

[6] Benjamin Liu, Alexander Sonn, Anthony Roy, and Brian Brewington. Deep learning method for heliostat instance segmentation. *SolarPACES Conference Proceedings*, 1, Feb. 2024.

[7] Lalit Singh Parmar and Sudhir Kumar Singh. A study of performance and analysis csp renewable based on solar tower power plant. In *2022 5th International Conference on Contemporary Computing and Informatics (IC3I)*, pages 1094–1099, 2022.

[8] Saeid Shokri, Reza Hayati, Mahdi Ahmadi Marvast, Ayazi Mohammad, and Ganji Hamid. Real time optimization as a tool for increasing petroleum refineries profits. *Petroleum and Coal*, 01 2009.

[9] Michael Soderstrand, Sung Lee, and Peter Chung. Mini-dish based hybrid concentrated solar power (csp) system for home use. pages 689–692, 08 2013.

[10] David B. Thomas and Wayne Luk. Sampling from the multivariate gaussian distribution using reconfigurable hardware. In *15th Annual IEEE Symposium on Field-Programmable Custom Computing Machines (FCCM 2007)*, pages 3–12, 2007.

[11] W.T. Xie, Y.J. Dai, R.Z. Wang, and K. Sumathy. Concentrated solar energy applications using fresnel lenses: A review. *Renewable and Sustainable Energy Reviews*, 15(6):2588–2606, 2011.

[12] Lingxiang Yao, Yang Wang, and Xianyong Xiao. Concentrated solar power plant modeling for power system studies. *IEEE Transactions on Power Systems*, 39(2):4252–4263, 2024.